

ORIGINAL ARTICLE

Open Access



Application of machine learning technique for dynamic analysis of confined geomaterial subjected to vibratory load

Ammu Boban¹ , Preeti Pateriya^{1*} , Yakshansh Kumar¹ , Kshitij Gaur¹ and Ashutosh Trivedi¹

Abstract

Computer programming-based numerical programs are firmly established in geotechnical engineering, with rapid growth of finite element modeling and machine learning techniques gaining much attention both in practice and academia. This study is intended to expedite the dissemination of advanced computer applications in terms of finite element simulation and machine learning models by investigating the dynamic response of geomaterials subjected to vibratory loads. Several trial models were built to perform the experimental investigations with a vibratory shaker, signal generator, several accelerometers, a data collection system, and other ancillary devices. The implicit integration techniques in commercialized software were adopted for numerical simulations. After data collection from numerical simulation, models were chosen, trained, and assessed to produce predictions that were then used in this study. Several technologies, including the ensemble boosted tree, squared exponential Gaussian Process Regression (GPR), Matern 5/2 GPR, exponential GPR, and decision tree architectures (fine and medium), were used to forecast the displacement of confined geomaterial. The displacement-depth ratio was found rising to 80% in the frequency range of 5 to 25 Hz, suggesting a considerable change in the behavior of the geomaterial. The Matern 5/2 GPR model showed better accuracy with an R^2 value of 0.99, indicating an outstanding predictive ability. The Matern 5/2 GPR and boosted tree models could help better understand the links between displacement and its distribution along the direction of load application. The outcomes of this study based on computer-aided finite element programs can be effectively implemented in machine learning to develop computer programs. In conclusion, the computational machine learning models adopted in this study offer a new insight for uncovering hidden intrinsic laws and creating new knowledge for geotechnical researchers and practitioners.

Keywords Machine learning technique, Dynamic analysis, Confined geomaterial, Vibratory load

1 Introduction

Numerous studies have been conducted on scenarios of dynamic stresses, including traffics, seismic loads, machine foundations, and piling, and the results can be applied in the field of clay or sandy soils. Various testing methods have been implemented to ascertain the

dynamic properties of various soils, with focuses on sand, so as to find relationships among shear stiffness, damping ratio, and stiffness (Gupta & Trivedi, 2009; Ishibashi & Zhang, 1993; Ojha & Trivedi, 2013; Seed et al., 1986; Kumar et al., 2023a, 2023b; Mohan et al., 2021). The shaking table test and centrifuge test are most commonly used (Alshawmar & Fall, 2022). Machine learning techniques, including Category Theory and Regression Artificial Neural Networks (ANN) with Random Forests (CRRF), have been employed to forecast sand secant shear modulus and damping ratio (Baghbani et al., 2023). The models demonstrated high accuracy (R values of

*Correspondence:

Preeti Pateriya

preetipateriya_2k21phdce503@dtu.ac.in

¹ Department of Civil Engineering, Delhi Technological University, Delhi, India



© The Author(s) 2024. **Open Access** This article is licensed under a Creative Commons Attribution 4.0 International License, which permits use, sharing, adaptation, distribution and reproduction in any medium or format, as long as you give appropriate credit to the original author(s) and the source, provide a link to the Creative Commons licence, and indicate if changes were made. The images or other third party material in this article are included in the article's Creative Commons licence, unless indicated otherwise in a credit line to the material. If material is not included in the article's Creative Commons licence and your intended use is not permitted by statutory regulation or exceeds the permitted use, you will need to obtain permission directly from the copyright holder. To view a copy of this licence, visit <http://creativecommons.org/licenses/by/4.0/>.

0.998 for ANN and 0.995 for CRRF), highlighting the significance of relative density, vertical stress, and cyclic stress ratio in predicting dynamic characteristics.

In contrast, traditional backpropagation methods (such as MRM and MLP) are outperformed by the Adaptive Network-based Fuzzy Inference System (ANFIS), which can be used for superior modeling for soil parameters (Akbulut et al., 2004). ANN-DFO (Artificial Neural Network-Dragonfly Optimizer), an innovative hybrid model, excels in forecasting displacement amplitudes under vibration loading, with its result surpassing RF, GPR, and M-5 rules (Hasthi et al., 2022). Sensitivity analysis has identified crucial input variables. Genetic programming and ANN have been employed to create predictive formulas for displacement amplitudes, with the former outperforming the latter, highlighting the impact of the operating frequency (Sharma et al., 2019). For the seismic investigation of soil-pile-structure (SPS) systems, a data-based model with two hidden layers has successfully anticipated dynamic properties and seismic responses, demonstrating the practical potential of data-based techniques (Farfani et al., 2015). A dual-driven approach combining Scoops 3D for physics-informed qualitative assessment and the random forest algorithm for data-driven landslide susceptibility analysis has significantly boosted the model performance, as showcased by a 20.1% increase in the area under the receiver operating characteristic curve (AUC), revealing the effectiveness of integrating qualitative and quantitative factors (Liu et al., 2023). In geotechnical engineering, Feedforward Neural Networks (FNN) is widely used, but the limited improvement potential of deep FNN compromises its adoption. Recurrent Neural Networks (RNN), especially with Long Short-Term Memory (LSTM), excels in addressing time series problems, such as landslide deformation prediction. Convolutional Neural Networks (CNN) are effective for image-processing tasks, like porous media reconstruction. Although Generative Adversarial Networks (GAN) are relatively new in geotechnical applications, their potential lies in complementing other supervised learning algorithms, due to their excellent generating ability (Phoon et al., 2023; Zhang et al., 2021; Zhang et al., 2022). Although the existing literature has illustrated the utilization of Machine Learning (ML) in geotechnical studies, there is a noticeable gap in the explicit exploration of ML techniques in soil displacement analysis under vibratory loads. Given substantial risks associated with geohazards or structural failures, increasingly more emphases are placed on evaluating the safety of geotechnical structures, since geohazards or structural failures would pose significant threats to human's lives and properties. As a result, there is a research gap in this field, which is yet to be filled. However, numerous difficulties

may arise when ML is used to predict soil displacement caused by vibratory stress. It is not easy to find out high-quality datasets with various soil qualities, input parameters, and associated displacement measurements under vibratory loading circumstances. But such datasets are required for training and validating ML models properly. Furthermore, it is still difficult to comprehend and explain ML models in geotechnical engineering. In a word, interpretable ML models would advance the adoption of ML techniques by the geotechnical engineering community, since they can offer valuable insights into the underlying soil behavior.

This study used an accelerometer to determine the acceleration, velocity, and displacement over a range of distances. Accelerometer is composed of electromechanical sensors that can produce electrical charges proportional to the force exerted. Some geomaterial confined in a steel tank was excited at varied frequencies, while the accelerometer captured the data. Accelerometer signals were then measured in a data acquisition system which logged both static and dynamic activities. In this study, the models adopted to perform the machine learning investigations include the fine and medium decision-tree structures, the Matern 5/2 GPR, the rational quadratic GPR, the squared exponential GPR, the exponential GPR, and the boosted tree. The strength of adaptive learning was used to achieve more precise parameter estimation. Such precision is crucial in applications where accurate modeling of system behavior is necessary. Traditional backpropagation methods, especially when used in deep learning, are sensitive to the initialization of weights. However, ANFIS, a hybrid approach, exhibits reduced sensitivity to such initialization issues, thus becoming a more robust and easier method for training effectively. The novelty of this study lies in the integration of machine learning techniques for dynamic analysis of confined geomaterial subjected to dynamic load, delivering advancement in an interdisciplinary approach to explore the frequency-dependent behavior of displacement. Moreover, the models can effectively facilitate the understanding of the dynamics of confined geomaterial and the designing of such structures as machine foundations, pavements, railway tracks, etc.

2 Materials and methods

2.1 Properties of confined geomaterial

The grain size distribution curve gives a poorly graded sand (SP). According to IS 2720-4 (1985), the uniformity coefficient (C_u) is 2.31 and the curvature coefficient (C_c) is 0.94 (Fig. 1a). Based on IS 2720-7 (1980), the standard proctor compaction curve with the moisture content and maximum dry density are shown in Fig. 1b. The angles

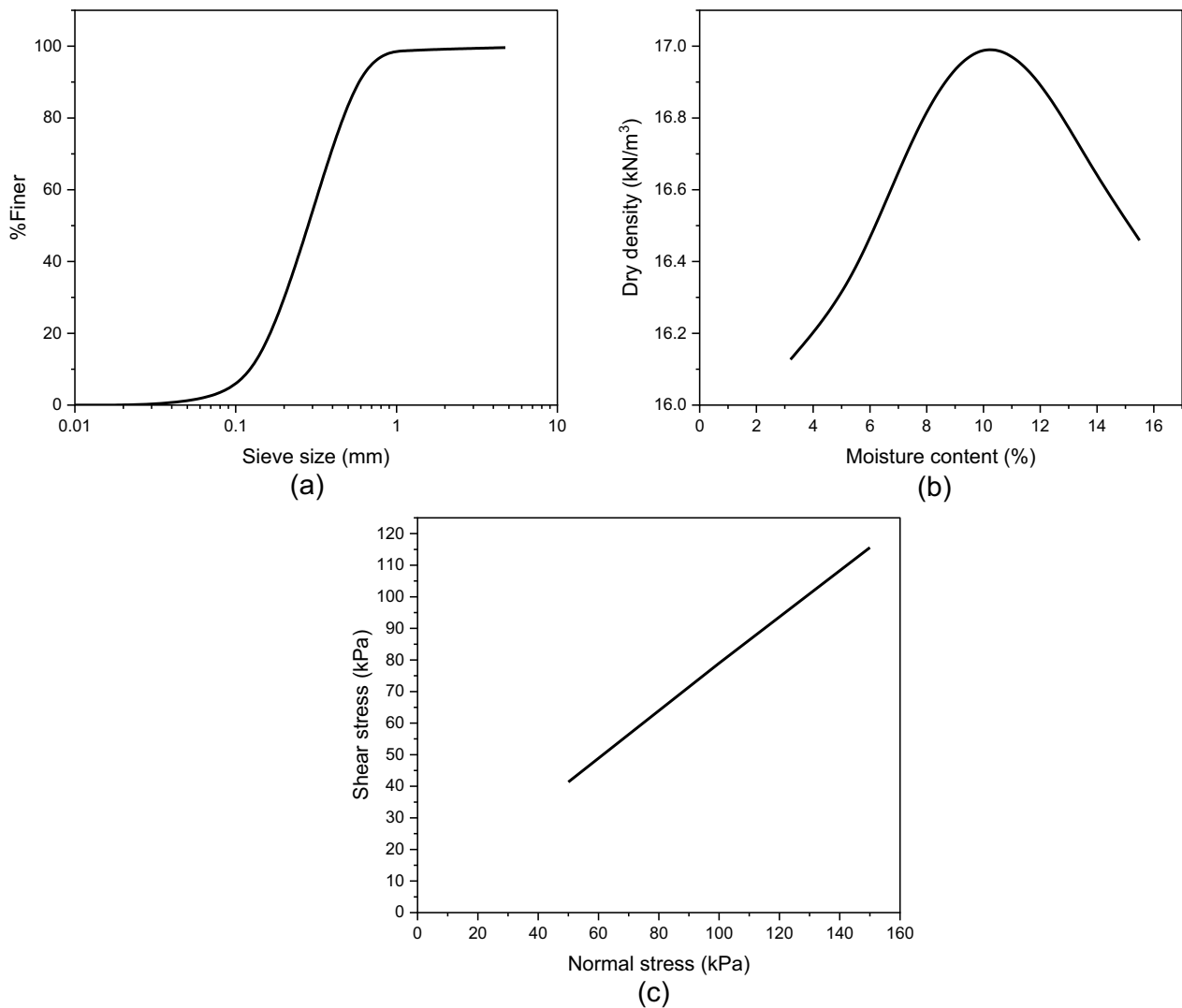


Fig. 1 Geomaterial properties: (a) grain size distribution curve, (b) standard proctor compaction curve, and (c) shear stress vs. normal stress curve

of internal friction and cohesion are evaluated utilizing shear stress vs. normal stress plot as shown in Fig. 1c (IS 2720-13, 1986).

The properties of the confined geomaterial surveyed in this study are shown in Table 1.

2.2 Experimental program

Experiments were set up to evaluate the response of the controlled geomaterial subjected to dynamic load. The displacement response of the controlled geomaterial was evaluated along the depth. The experimental test setup includes a steel tank with a volume of 600 mm×460 mm×400 mm, filled with the geomaterial, as shown in Table 2.

Table 1 Properties of the confined geomaterial

Properties	Results
Geomaterial classification	Poorly graded sand (SP)
Specific gravity (G_s)	2.68
Optimum moisture content (OMC)	10.4%
Maximum dry unit weight (MDU)	17 kN/m ³
Cohesion (c)	4.4 kPa
Peak friction angle (ϕ_p)	36.59°

The diagrammatic representation of Fig. 2a, b shows the arrangement of accelerometers, along with a power amplifier cum signal generator, an electrodynamic

Table 2 Geomaterial parameters used in the numerical analysis of this study

Parameters	Magnitude
Poisson's ratio (μ)	0.45 ^a
Young's modulus, E (MPa)	30–50 ^a
Dilation angle (ψ_D)	1°
Constant volume friction angle (ϕ_c)	35°
Unit weight, γ (kN/m ³)	18

^a Kumar et al. (2023)

vibratory shaker, a steel tank filled with geomaterial, and a digital vibration meter. The testing configuration includes a dynamic vibrator (MEV-0020 electrodynamic vibrator), a data recorder, and several accelerometers (Kumari & Trivedi, 2022, 2020b, 2020c; Singh et al., 2020a). The accelerometers are strategically placed at a width of 5, 10, 15, 20 cm, respectively inside the tank as shown in Fig. 2b.

The accelerometers are mounted on a steel plate, so as to ensure stability and accurate measurement of vibrations, which are generated by an MEV-0020 electrodynamic vibrator. This vibrator consists of a moving platform, which is positioned to strike the steel tank with the geomaterial from the sides. The power amplifier cum signal generator (MPA-0500) is used to drive the electrodynamic vibrator. The vibrator is excited at the frequencies of 5, 10, 15, 20, and 25 Hz, which are chosen to cover the range of vibrations often encountered in real-world scenarios. The accelerometers measure the displacement, velocity, and acceleration of the granular substance at different depths. The

displacement data are logged by an MVM-555 digital vibration meter, which can record vibration-induced position changes over time. When the vibrator strikes the steel tank, vibrations would be caused in the geomaterial. The accelerometers would then collect data on the displacement velocity, and acceleration of the geomaterial at various depths in response to the applied vibrations. Throughout the experiment, the data recorder would monitor and record the measurements taken by the accelerometers. After the experiments are completed, the collected data will be analyzed, so as to understand how the vibrations induced by the electrodynamic vibrator at different frequencies have impacted the displacement, velocity and acceleration of the geomaterial at various depths. A flowchart representing the dynamic displacement prediction model developed for confined geomaterial subjected to vibratory load is as shown in Fig. 3.

2.3 Numerical analysis

Numerical analysis was performed with computational software of Abaqus /CAE (2017). The computational program considered a peak value of the angle of internal friction, ϕ_p , where, $\phi_p = \phi_c + \psi_D$, which is a function of the constant volume friction angle, ϕ_c , and the angle of dilation, ψ_D (Mehra & Trivedi, 2021). The input parameters for the geomaterial medium are defined in Table 1. The steel tank was filled with geomaterial, and the boundary conditions considered were fixed at the exterior surface, in order to model the confinement of the geomaterial. The four-node plane stress element (CPS4R), with reduced integration, was considered for

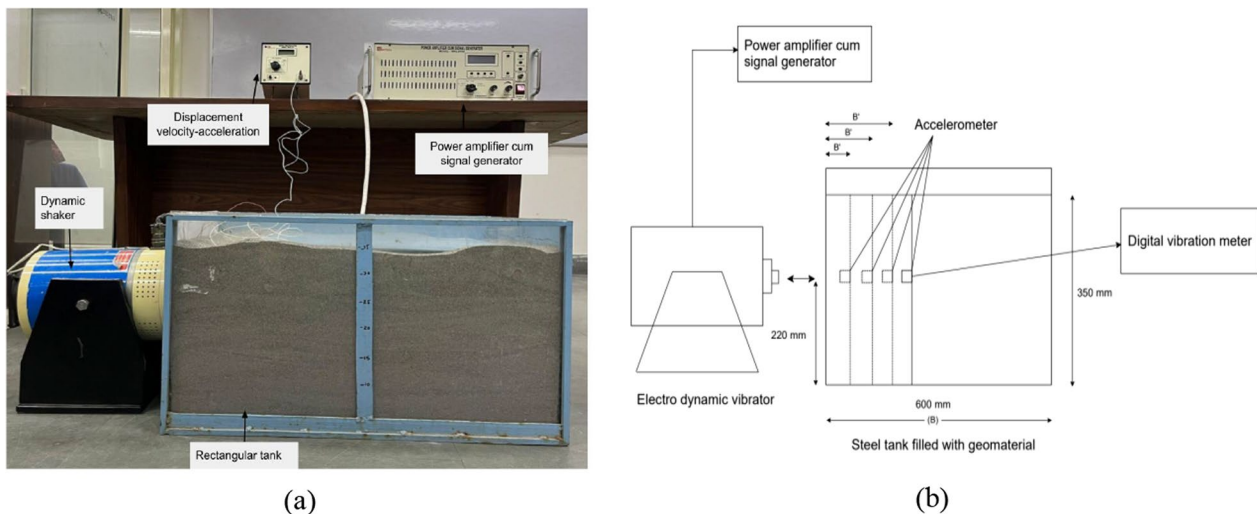


Fig. 2 a Experimental setup b Diagrammatic representation. They show the arrangement of accelerometers along with a power amplifier cum signal generator, an electrodynamic vibratory shaker, a steel tank filled with geomaterial, and a digital vibration meter

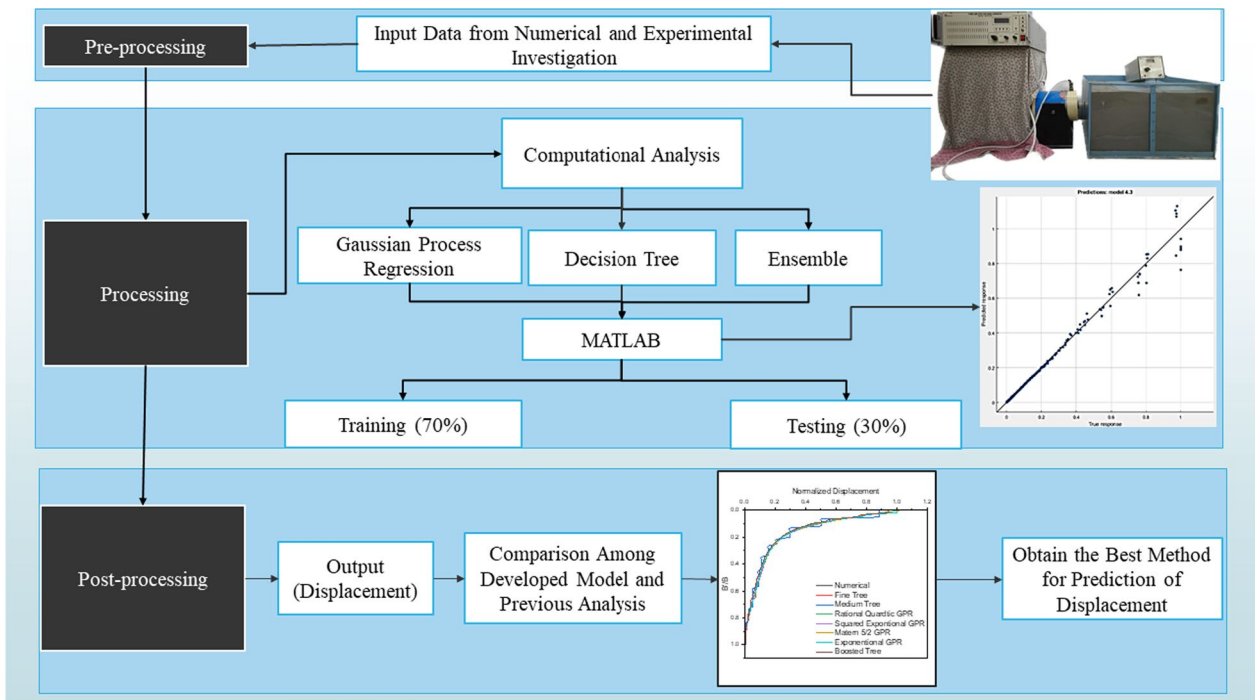


Fig. 3 Flow chart of the dynamic displacement prediction model developed for confined geomaterial subjected to vibratory load

numerical modeling. The top surface was considered unconfined for the numerical analysis. Dynamic load was applied to the tank’s side walls at varied frequencies, i.e., 5–25 Hz. The parameters of the geomaterial for the present numerical analysis are shown in Table 2.

2.4 Machine learning approach

The data acquired in the experimental investigation were used to validate the numerical model, while the numerical analysis was made to determine various data, including: tank width, particle size corresponding to D_{50} , density, pressure applied by the armature, and loading frequency, which were inputted for the data training set in the machine learning model. Thereafter, the input parameters are normalized to clean the dataset for the machine learning model. This is followed by the selection parameter step, where the input variables influencing the displacement of confined geomaterial were selected from numerical investigation. Subsequently, a machine learning algorithm was obtained from numerical analysis and the target variable (displacement). The model was then trained to create a training set and a testing set based on the dataset, followed by a model evaluation step, where the testing set would evaluate the trained model. The accuracy of the model’s prediction of displacement can be assessed with the mean squared error (MSE), root mean squared error (RMSE), mean absolute error (MAE), and

coefficient of determination (R^2). Equations below are used to determine R^2 , RMSE, MAE, and MSE. (1–4) (Ahmad et al., 2018; Ibrahim et al., 2022; Younas et al., 2022).

$$R = \frac{n \sum (xy) - (\sum x)(\sum y)}{\sqrt{(n \sum x^2 - (\sum x)^2)(n \sum y^2 - (\sum y)^2)}} \quad (1)$$

$$RMSE = \sqrt{\frac{\sum_{i=1}^n (y_i - \hat{y}_i)^2}{n}} \quad (2)$$

$$MAE = \frac{1}{n} \sum_{i=1}^n |\hat{y}_i - y_i| \quad (3)$$

$$MSE = \frac{1}{n} \sum_{i=1}^n (y_i - \hat{y}_i)^2 \quad (4)$$

where x and y indicate the input and output parameters for the dataset with n sample points, respectively; \hat{y}_i and y_i are the predicted and actual values, respectively.

Prediction—After trained and evaluated, the model would be used to forecast displacement for the untested samples. When relevant sand parameters are provided, the model will generate displacement estimates.

2.5 Machine learning models

2.5.1 Decision tree

Decision Tree (DT) is used to classify an unknown sample into several groups by successively applying one or more decision functions (Swain & Hauska, 1977). The classifier adopted in this process is a tree structure with leaf nodes, which represent classification results, and inner nodes, which represent dataset features, branching, and decision-making processes. The DT approach can break down complex problems into simple ones, resulting in an easy-to-understand solution (Xu et al., 2005). Based on dataset features, a test or decision can be finally made.

Let x represent the pattern or feature vector; Y (which takes integer values) is defined as the class label that has been assigned to take values from the real-valued space R_q . The $d(\cdot)$ decision rule function maps the elements in R_q to the matching class label Y (Safavian & Landgrebe, 1991), and the valid misclassification rate of d can be expressed as below:

$$R^*(d) = p(d(X) \neq Y) \quad (5)$$

Training a DT model involves employing recursive partitioning and multiple regressions on the training dataset. This process begins at the root node and repetitively splits data within each internal node according to a defined rule, until specific halting requirements are reached (Rodriguez-Galiano et al., 2015).

There are two scoring criteria, i.e., Information Gain (InfoGain) (Quinlan, 1993) and Gini Index (Gini) (Breiman, 1984).

$$\text{Info} = - \sum_j \left(\frac{N_j(t)}{N(t)} \right) \log_2 \left(\frac{N_j(t)}{N(t)} \right) \quad (6)$$

As shown, in node t , there are N_j samples, $N(t)$ samples, and $N_j(t)$ samples of class j . N_j is the total number of samples in node t .

$$\text{InfoGain} = \text{Info}(\text{parent}) - \sum_k (p_k) \text{Info}(\text{child}_k) \quad (7)$$

where p_k denotes the percentage of samples sent to the k -th subspace, and $\text{Info}(q)$ denotes the information of the feature subspace q .

$$\text{Impurity} = 1 - \sum_j \|p(j)N_j(t)/N(t)\|^2 \quad (8)$$

$$\text{Gini} = \text{Impurity}(\text{parent}) - \sum_k (p_k) \text{Impurity}(\text{child}_k) \quad (9)$$

$p(j)$ denotes the prior probability that a sample belongs to class j for a set of training samples, and $\|g\|$ denotes the normalization of the vector g to unit length. To match the default configuration in the Matlab decision tree code, proportional priors are used, i.e., $p(j) = N_j/N(1)$ (Myles et al., 2004).

Three alternative DT topologies are accessible in this situation. The first architecture is made up of “Fine” DT, the most sophisticated of the three. The second architecture is labeled as “Medium”, while the third as “Coarse”.

2.6 Gaussian process regression

Vector data points are represented by $D=y(xi): I=1\dots n$, where x is any input variable. The expected value $E[y(x) | x, D]$ and the covariance $\text{cov}[y(x) | x, D]$ are to be calculated for a test input x . The correlations between the noise and signal components of $y(x)$ vary with x . Assuming $x=t$, one element of the p -dimensional vector $y(t)$ may represent the level of expression of a certain gene at a particular time. The variances and correlations among these genes at time t , on the other hand, would be reflected in the other components (t). The entire vector $y(x)$ is modeled to reflect its interactions and dependencies, rather than assuming temporal dependence (Wilson et al., 2011).

$$y(x) = W(x)[f(x) + \sigma_f \epsilon] + \sigma_y z \quad (10)$$

ϵ represents a random variable, and z represents independent and identically distributed white noise following a Gaussian distribution with the mean 0 and identity covariance matrix ($\mathcal{N}(0, I)$). $W(x)$ is a $p \times q$ matrix made up of independent Gaussian Processes (GPs), whereas $f(x) = (f_1(x), \dots, f_q(x))^T$ is a $q \times 1$ vector made up of independent GPs (Quinonero-Candela & Rasmussen, 2005).

A collection of random variables, known as a GP, has joint Gaussian distributions that are valid for all finite numbers. The Matérn 5/2 GPR, rational quadratic GPR, squared exponential GPR, and exponential GPR are some examples of GPR models. Among them, the rational quadratic GPR kernel is particularly useful for showing data with fluctuations of various magnitudes; therefore, it has been widely utilized in multivariate statistical analysis in metric spaces, geostatistics, machine learning, and spatial statistics (Zhang et al., 2018). In the context of function space, the squared exponential GPR represents a regression model with an unlimited number of basis functions, similar to a radial basis function regression model; and it can be distinguished from the exponential GPR by squaring the Euclidean distance. One distinctive quality of the squared exponential GPR is the use of kernels to replace inner products of basis functions (Athavale et al., 2019). The Matérn 5/2 kernel generates Fourier transforms of the Radial Basis Function (RBF)

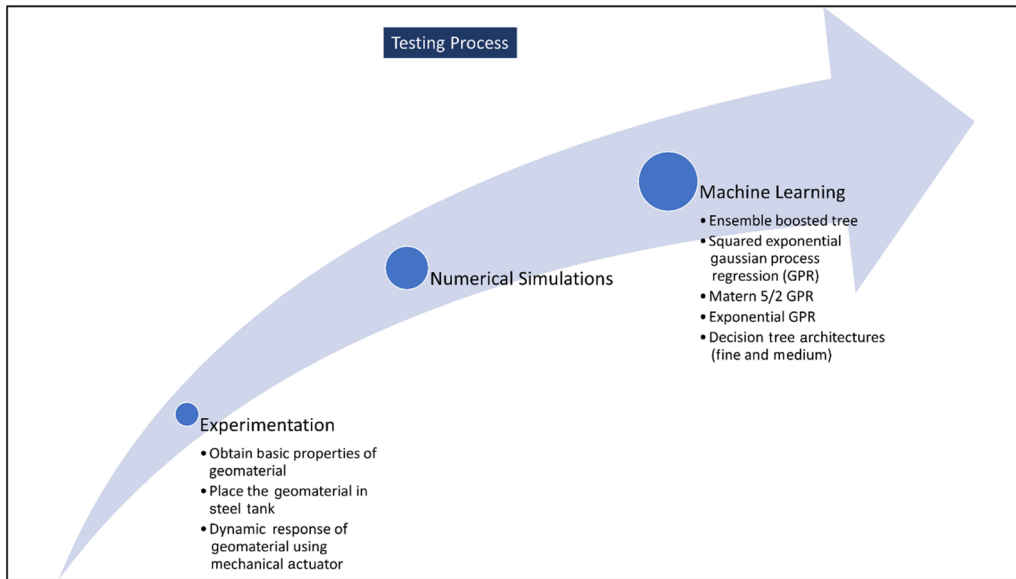


Fig. 4 The testing process of this study

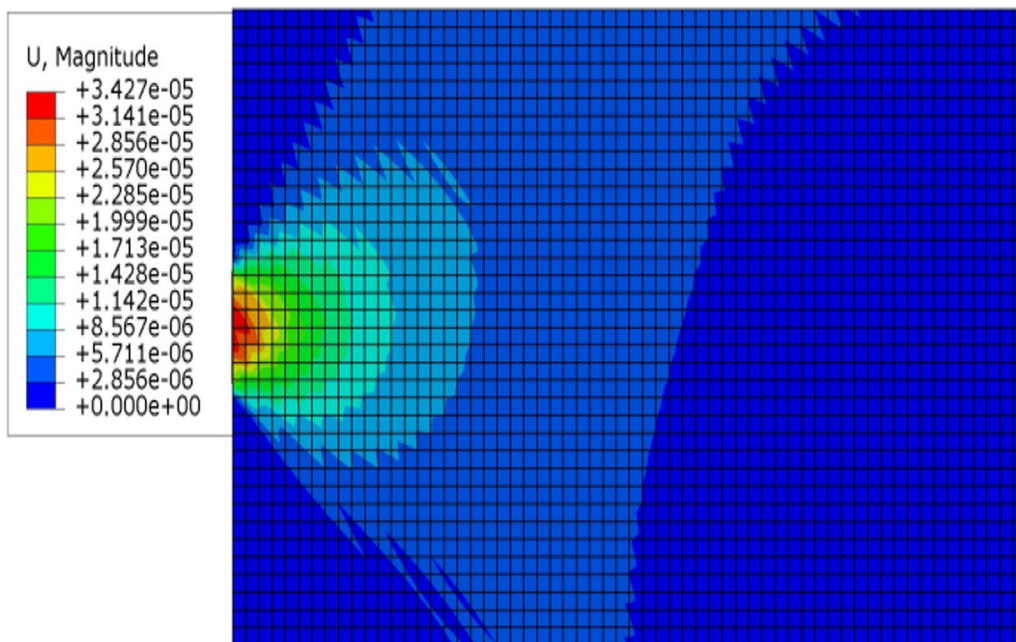


Fig. 5 Geomaterial's sectional view. The color scheme is selected to illustrate the magnitude of displacement: red and blue colors are for the maximum (3.427×10^{-5}) and minimum (2.856×10^{-06}) displacement, respectively

kernel from spectral densities of the stationary kernel; it can avoid high-dimensional concentration of measure problems. Modeling data in such spaces is suitable (Li et al., 2021). The exponential GPR uses kernels, instead of basis function inner products; although it may struggle to detect abrupt data discontinuities, it can accurately approximate smooth operations.

Ensemble machine learning can be used to create a flawless prediction model from several basic models. The classifiers categorize new data points by voting with or without weights (Dietterich, 2000). These methods have solved several machine-learning problems. Then, a methodology for training many models and integrating their predictions is adopted to improve predictive

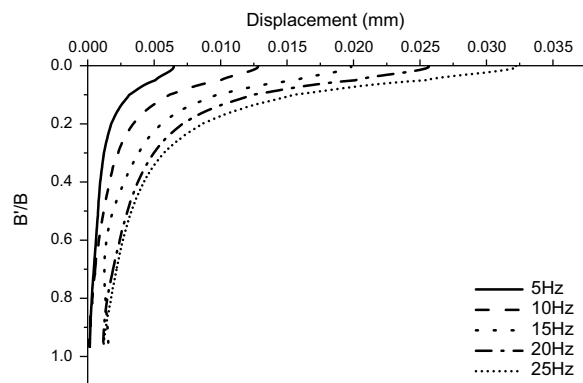


Fig. 6 Variation of displacement with B/B' (where B and B' denote the breadth of the steel tank and the width at which the displacement was measured, respectively) in the frequency range of (5–25) Hz at $\gamma = 18 \text{ kN/m}^3$

performance (Sagi & Rokach, 2018). Based on the variety and experience of multiple models, Ensemble techniques can handle complex patterns, reduce overfitting, and increase generalization. This approach is fundamental to modern machine learning, because it succeeds across numerous domains. Afterwards, the averaging of the forecast from each decision tree is done, a process called “bagging”, followed by a process called “boosting”, which successively adds ensemble members that give correct predictions generated by previous models, while producing a weighted average of the predictions. Focused on improperly classified samples, this process repeatedly changes sample weights to improve the classification abilities of basic models during the integration stage (Dong et al., 2020). The experiment as described above was carried out with the classification toolbox in MATLAB. To predict soil displacement under vibratory pressure, this study developed fine and medium decision tree structures, Matern 5/2 GPR, rational quadratic GPR, squared exponential GPR, exponential GPR, and boosted tree models.

The step-by-step testing procedure of this study is detailed below:

2.7 Step 1: experimentation

- The testing configuration includes a dynamic vibrator (MEV-0020 electrodynamic vibrator), a data recorder, and several accelerometers (Kumari & Trivedi, ; Singh et al., 2020a). The accelerometers are strategically placed at various depths inside the tank.
- The experiments were performed in a controlled environment to observe the properties of geomaterial

by using the direct shear test, pycnometer, and standard proctors test.

- After the basic properties of geomaterial listed in Table 1 were obtained, the geomaterial was then placed in a steel tank, with a mechanical actuator used to investigate the dynamic response of confined geomaterial.
- The diagrammatic representation of Fig. 2a, b shows the arrangement of the accelerometers along with the power amplifier cum signal generator, electrodynamic vibratory shaker, geomaterial-filled steel tank, and digital vibration meter; and a flow chart is shown below.

2.8 Step 2: numerical simulation

- Numerical simulations were carried out in a set of commercial finite element software (Abaqus/ CAE 2017).
- The properties, including angle of friction, cohesion and unit weight, were inputted from the experimental test results.
- To perform the numerical simulations, such parameters as dilation angle, modulus of elasticity, and poisons ratio, are required, in addition to the properties listed above and inputted in the model as per the range provided by Kumar et al. (2023).
- Using implicit integration, the numerical simulations were carried out for the dynamic response of confined geomaterial subjected to dynamic loads.

2.9 Step 3: implementation of machine learning

- Based on the data acquired from the numerical simulations, several machine learning models, including Ensemble boosted tree, Squared exponential Gaussian Process Regression (GPR), Matern 5/2 GPR, Exponential GPR, and Decision tree architectures (fine and medium), were used to make predictions of displacement and a possible implementation for a computer program.

3 Results and discussion

3.1 Experimental and numerical programs

The testing process employs experimentation, numerical simulation and machine learning utilized in this study (Fig. 4). The numerical modeling results and the ML model's forecast are compared for each input parameter considered in this study. The accelerometers are placed at

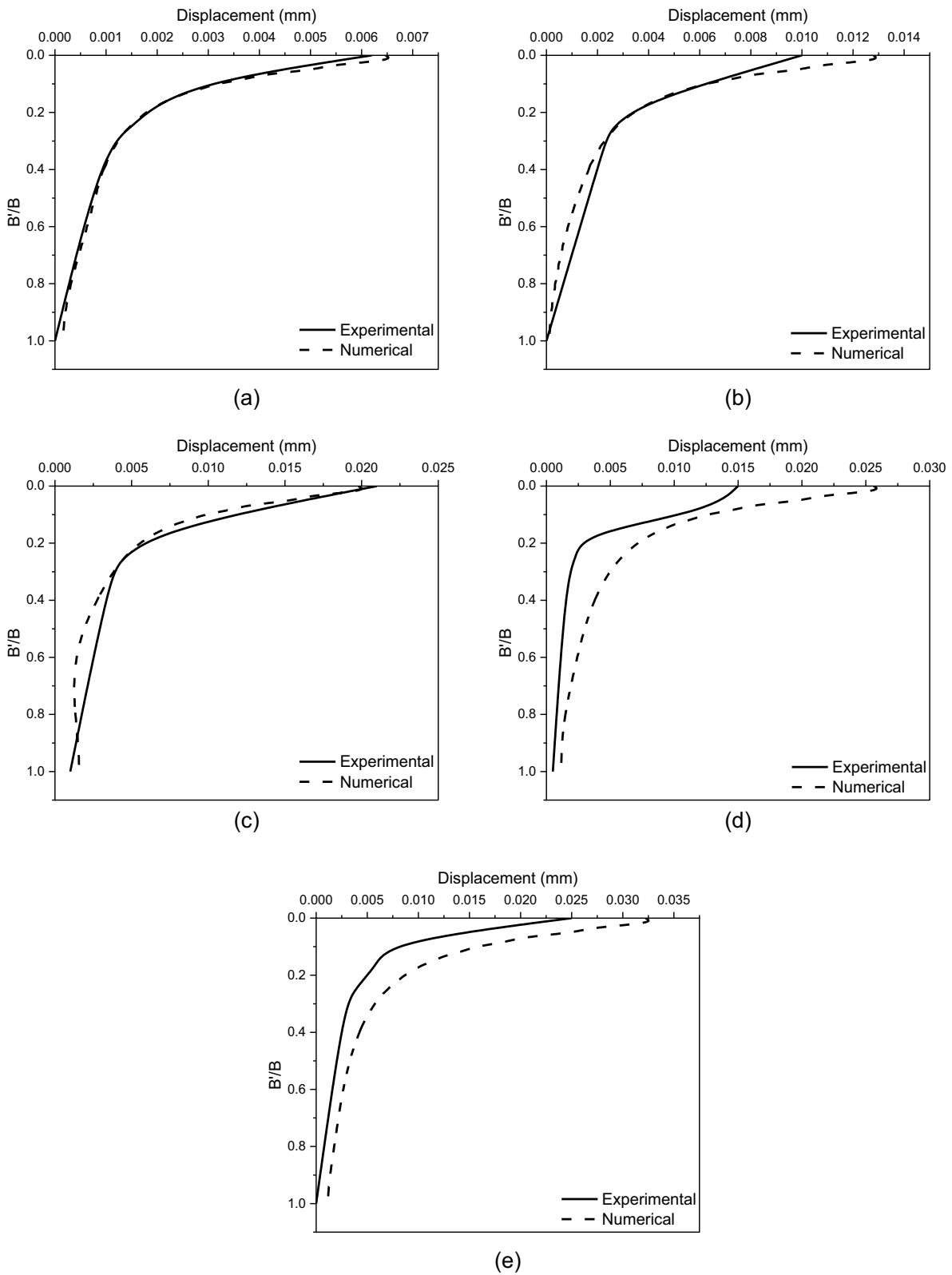


Fig. 7 Variation of geomeaterial displacement with the depth as captured at frequencies of (a) 5 Hz, (b) 10 Hz, (c) 15 Hz, (d) 20 Hz, and (e) 25 Hz. The outcomes from the numerical analysis are validated with the experimental observations

Table 3 Comparison of models' performance

Model	RSME	R ²	MSE	MAE
Fine tree	0.031891	0.98	0.0010171	0.019795
Medium tree	0.071315	0.91	0.0050858	0.036892
Rational Quadratic GPR	0.030544	0.98	0.00093291	0.010344
Square exponential GPR	0.032592	0.98	0.0010622	0.011338
Matern 5/2 GPR	0.028357	0.99	0.00080412	0.0091226
Exponential GPR	0.039679	0.97	0.0015745	0.011376
Boosted tree	1.32×10^{-6}	0.94	1.7424×10^{-12}	5.07×10^{-12}

varying distances from the shaking equipment to record the dynamic response of the geomaterial. The geomaterial's sectional view is shown in Fig. 5. The color scheme is selected to illustrate the magnitude of displacement: red and blue colors are for the maximum (3.427×10^{-5}) and minimum (2.856×10^{-6}) displacement, respectively. As seen, the displacement decreases as the waves move away from the vibratory source. The outcomes from the ML modeling are in good agreement with the experimental and numerical results. The variation of displacement with B'/B (where B and B' denote the breadth of the steel tank and the width at which the displacement was measured, respectively) in the frequency range of (5–25) Hz at $\gamma = 18 \text{ kN/m}^3$ as shown in Fig. 6.

The variation of geomaterial displacement as captured at frequencies of (a) 5 Hz, (b) 10 Hz, (c) 15 Hz, (d) 20 Hz, and (e) 25 Hz is shown in Fig. 7a–e. The outcomes from the numerical analysis are validated with the experimental observations, so a good agreement has been achieved. The displacement is observed to increase with the frequency, but to decrease with the depth of the geomaterial. These models can be used to compute geomaterial's dynamic properties, such as shear modulus and damping ratio. The data were analyzed with fine and medium DT topologies, Matern 5/2 GPR, rational quadratic GPR, squared exponential GPR, exponential GPR, and boosted tree. The response plot shows the projected response with the recorded numbers after the regression model was trained. Hold-out or cross-validation predicts using a model learned without the associated observation. This study uses two-fold cross-validation. The feedforward and back-propagation network was trained in a backpropagation training algorithm. The input variables included: tank width (0–0.6 m), frequency (5–25 Hz), D50 (0.285), unit weight (18 kN/m^3), OMC (10.4%) of the geomaterial, and amateur pressure (30 kPa). The plot of the predicted vs. true responses for (a) fine tree, (b) medium tree, (c) Matern 5/2 GPR, (d) squared exponential GPR, (e) the rational quadratic GPR, (f) exponential GPR,

and (g) boosted tree is shown in Fig. 8a–g. The residual vs. true response plot of (a) fine tree, (b) medium tree, (c) Matern 5/2 GPR, (d) squared exponential GPR, (e) the rational quadratic GPR, (f) exponential GPR, and (g) boosted tree is shown in Fig. 9a–g. The model performance measures (RSME, R², MSE and MAE) are essential for analyzing the model efficacy. The performance of each model was assessed after the network was properly trained, with the results shown in Table 3. RMSE reflects the square root of the average of the squared differences between the actual and forecasted values in a regression model. RMSE is always positive, and cannot be negative, since, as indicated by its name, it gauges the average size of the errors. R² is a metric to show in what extent the dependent variable's variance can be accounted for by the independent variables in a model. This parameter ranges from 0 to 1, indicating whether a model can explain all variation or none. R-squared never exceeds 1. MAE is positive and less outlier-prone than RMSE.

To compare the displacement projections by the numerical and machine learning models, each model tested at 5–25 Hz is shown in Fig. 10. The mean squared error is used to evaluate the performance of a model. MSE presented for various models in this study indicates a better-performing model for an MSE ranging from 10^{-11} to 10^{-12} . The boosted tree model delivered the smallest MSE with a 1.7424×10^{-12} value. This exceptionally low value suggests that the boosted tree model gives the smallest overall prediction error. The boosted tree model for MAE further gives the lowest value of 5.07×10^{-12} , indicating that the boosted tree model can deliver the smallest average absolute difference between its predictions and the actual values. Hence, it is able to give better and more reliable results for developing machine learning-based computer software to predict displacement behavior, while designing structures resting on geomaterial subjected to dynamic loads.

4 Conclusions

By utilizing certain machine learning models, this study examined various forecasting approaches and assessed their efficiency. Several model experiments and numerical analyses were performed to evaluate the displacement of geomaterial along the width of a tank. Moreover, various machine learning models were effectively adopted to understand the dynamics of confined geomaterial. The main conclusions of this study are as follows:

- The displacement at different sections were kept relatively consistent along the width of confined geomaterial. However, as the frequency changes from 5 to 25 Hz, there was a significant increase in the peak

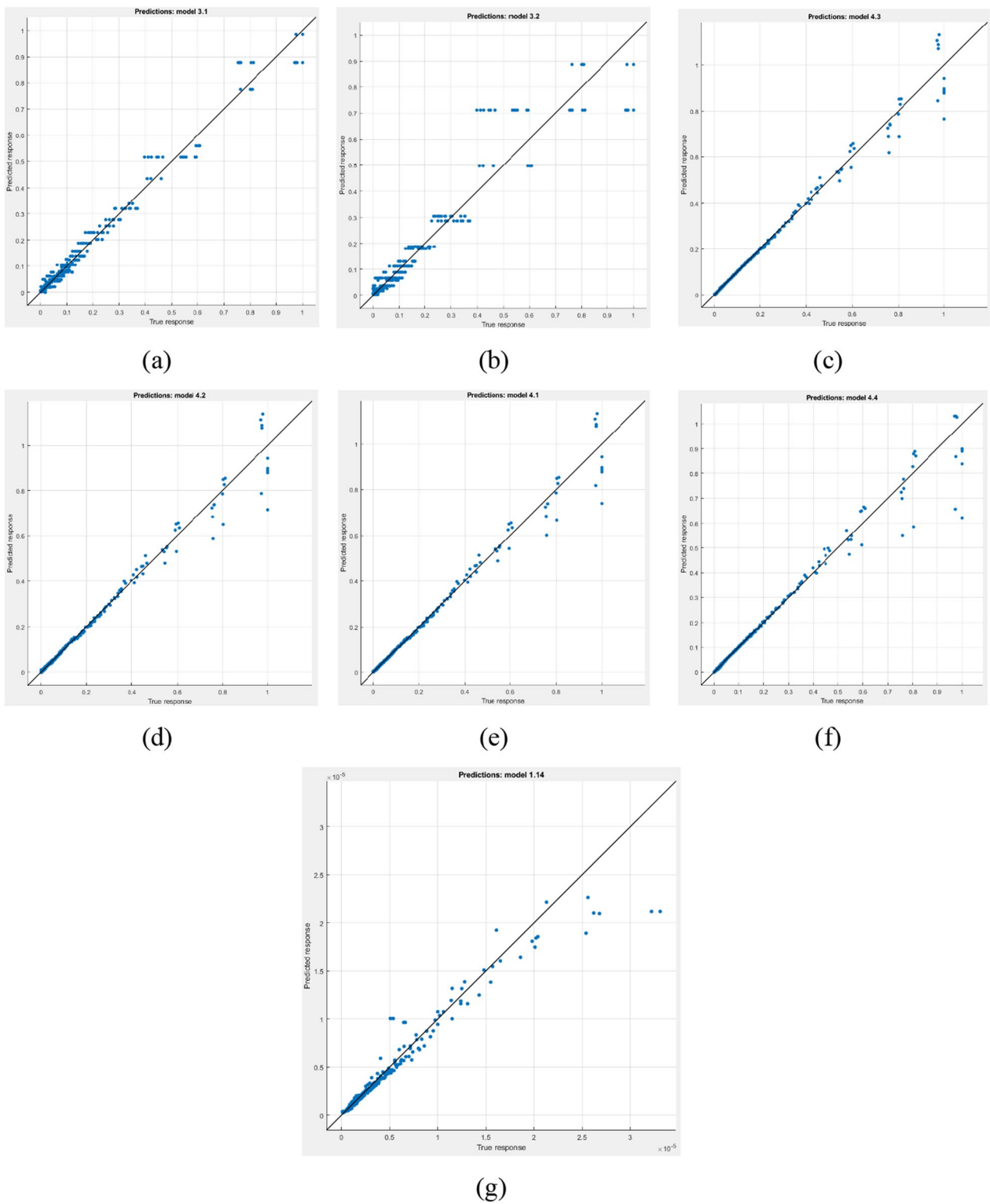


Fig. 8 The plot of the predicted vs. true responses of (a) fine tree, (b) medium tree, (c) Matern 5/2 GPR, (d) squared exponential GPR, (e) the rational quadratic GPR, (f) exponential GPR, and (g) boosted tree

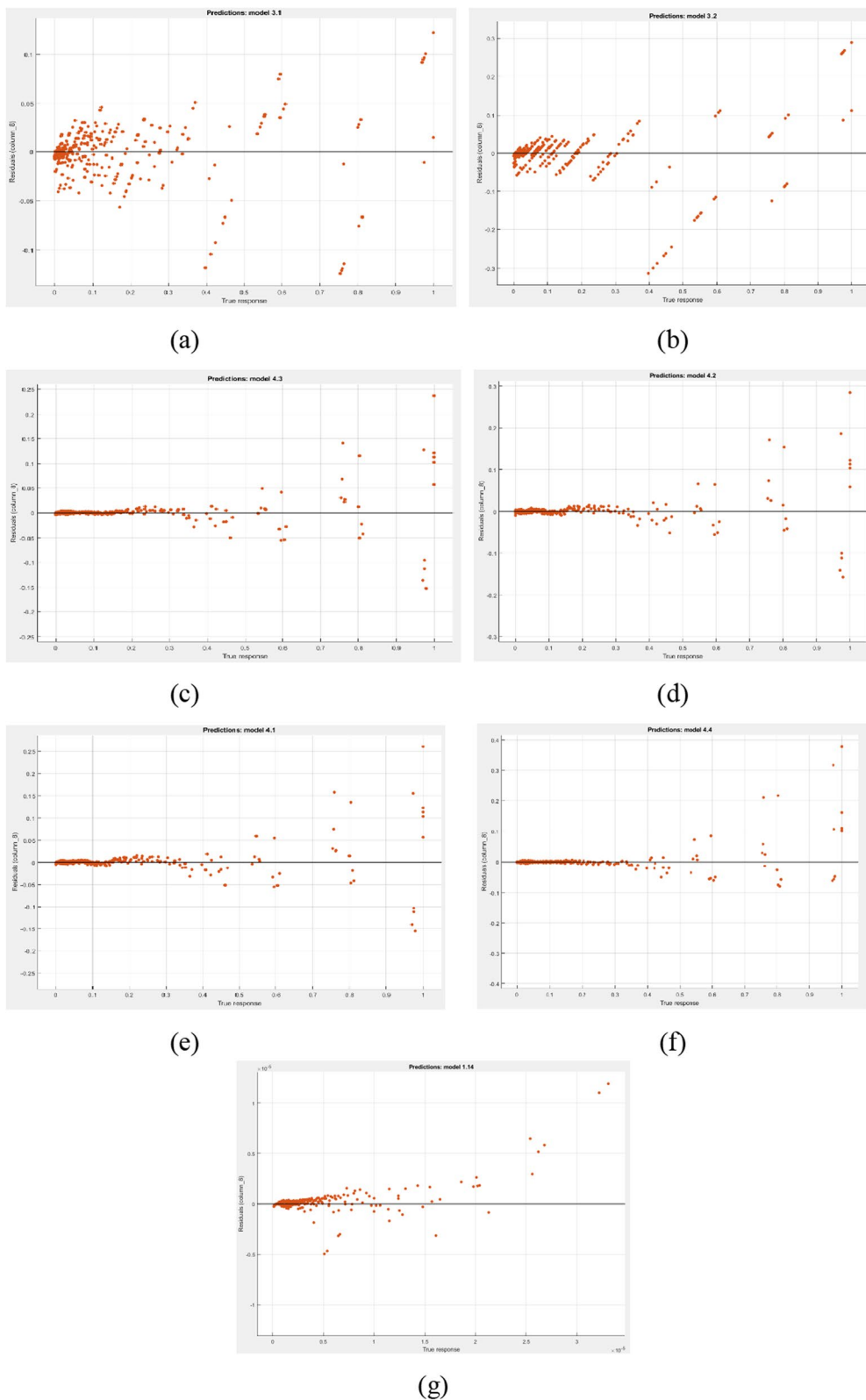


Fig. 9 The plot of the residual vs. true responses of (a) fine tree, (b) medium tree, (c) Matern 5/2 GPR, (d) squared exponential GPR, (e) the rational quadratic GPR, (f) exponential GPR, and (g) boosted tree

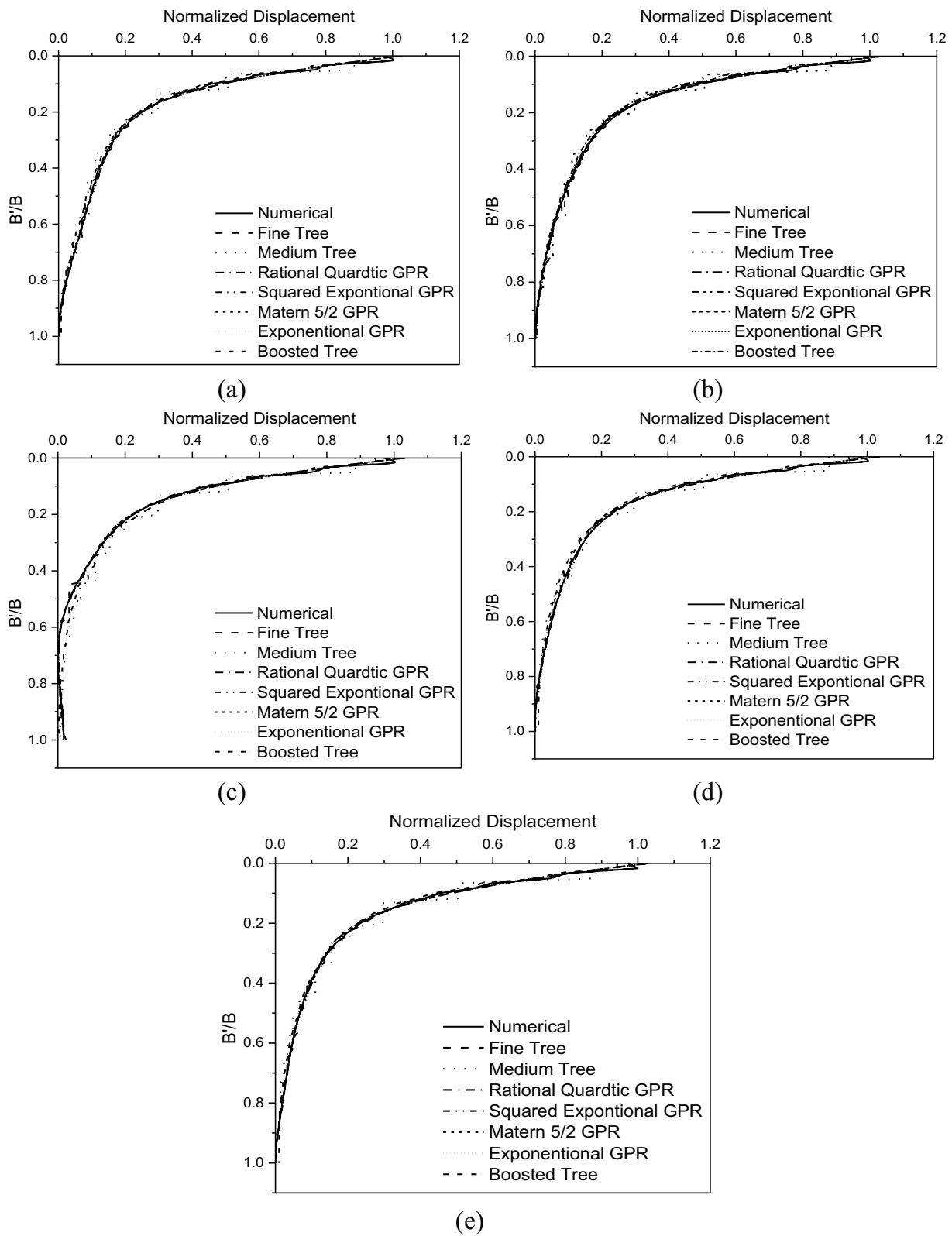


Fig. 10 Comparison of experimental and ML model results on displacement variation along the width ratio in (a) 5 Hz, (b) 10 Hz, (c) 15 Hz, (d) 20 Hz, and (e) 25 Hz

displacement from 0.006 to 0.03 mm. The highest peak displacement, identified at the frequency of 25 Hz, showcased an overall increase of 80% against the frequency of 5 Hz.

- The Matern 5/2 GPR model delivered the highest level of accuracy, as indicated by its greatest R^2 value of 0.99. Given that R^2 value measures the proportion of the variance in the dependent variable that is predictable from the independent variables, this greatest R^2 value indicates a strong relationship between the Matern 5/2 GPR model's prediction and the actual outcome. Therefore, based on this evaluation, the Matern 5/2 GPR model is considered the most reliable for accurate predictions.
- The mean squared error (MSE) is used as a performance metric for evaluating a model. MSE presented for varied models in this study indicates a better-performing model for an MSE ranging from 10^{-11} to 10^{-12} . The boosted tree model achieved the smallest MSE with a value of 1.7424×10^{-12} . This exceptionally low value suggests that the boosted tree model has the smallest overall prediction error.
- The boosted tree model for MAE further delivers the lowest value of 5.07×10^{-12} , indicating that this model has the smallest average absolute difference between its predictions and the actual values.

Abbreviations

GPR	gaussian process regression
CRRF	classification and regression random forests
ANN	artificial neural networks
ANFIS	adaptive network-based fuzzy inference system
MRM	multiple regression analysis method
MLP	multi-layer perceptrons
ANN-DFO	artificial neural network-dragonfly optimizer
RF	random forest
SPS	soil-pile-structure
ML	machine learning
MSE	mean squared error
RMSE	root mean squared error
MAE	mean absolute error
DT	decision tree
OMC	optimum moisture content
MDU	maximum dry unit weight
G	specific gravity
C	cohesion
Φ	friction angle
M	poison's ratio
E	young's modulus
Ψ_D	dilation angle
Γ	unit weight
R^2	coefficient of determination

Acknowledgements

The authors acknowledge the infrastructural support provided by Intelligent Transportation System and Soil Dynamic Laboratory at Department of Civil Engineering, Delhi Technological University, Delhi, India. Furthermore, the

support received under Project F. No. DTU/IRD/619/2105 of IRD DTU, Delhi, is thankfully acknowledged.

Author contributions

AB: Data collection, experimental analysis, and writing. PP: Machine learning analysis, writing, review, editing, and communication. YK: Numerical simulation, finite element analysis, writing, review, and editing. KG: Experimental analysis, review, and editing. AT: Conceptualization, supervision, final version, and proofreading.

Data availability

All data used to generate the models in this study appear in the submitted article.

Declarations

Conflict of interest

The authors declare no conflict of interest.

Received: 9 August 2023 Revised: 26 November 2023 Accepted: 28 December 2023

Published online: 01 February 2024

References

- Ahmad, M. W., Reynolds, J., & Rezgui, Y. (2018). Predictive modelling for solar thermal energy systems: A comparison of support vector regression, random forest, extra trees and regression trees. *Journal of Cleaner Production*, 203, 810–821.
- Akbulut, S., Hasiloglu, A. S., & Pamukcu, S. (2004). Data generation for shear modulus and damping ratio in reinforced sands using adaptive neuro-fuzzy inference system. *Soil Dynamics and Earthquake Engineering*, 24(11), 805–814.
- Alshawmar, F., & Fall, M. (2022). Geotechnical behaviour of layered paste tailings in shaking table testing. *International Journal of Mining, Reclamation and Environment*, 36(3), 174–195.
- Athavale, J., Yoda, M., & Joshi, Y. (2019). Comparison of data driven modeling approaches for temperature prediction in data centers. *International Journal of Heat and Mass Transfer*, 135, 1039–1052. <https://doi.org/10.1016/j.ijheatmasstransfer.2019.02.041>
- Baghbani, A., Choudhury, T., Samui, P., & Costa, S. (2023). Prediction of secant shear modulus and damping ratio for an extremely dilative silica sand based on machine learning techniques. *Soil Dynamics and Earthquake Engineering*, 165, 107708.
- Breiman, L. (1984). Olshen, and Stone. *Classification and Regression trees*.
- Dietterich, T. G. (2000). Ensemble methods in machine learning. In *Multiple Classifier Systems: First International Workshop, MCS 2000 Cagliari, Italy, June 21–23, 2000 Proceedings 1* (pp. 1–15). Springer Berlin Heidelberg.
- Dong, X., Yu, Z., Cao, W., Shi, Y., & Ma, Q. (2020). A survey on ensemble learning. *Frontiers of Computer Science*, 14, 241–258.
- Farfani, H. A., Behnamfar, F., & Fathollahi, A. (2015). Dynamic analysis of soil-structure interaction using the neural networks and the support vector machines. *Expert Systems with Applications*, 42(22), 8971–8981.
- Gupta, R., & Trivedi, A. (2009). Effect of non-plastic fines on the behavior of loose sand—An experimental study. *Electronic Journal of Geotechnical Engineering*, 14, 1–15.
- Hasthi, V., Raja, M. N. A., Hegde, A., & Shukla, S. K. (2022). Experimental and intelligent modelling for predicting the amplitude of footing resting on geocell-reinforced soil bed under vibratory load. *Transportation Geotechnics*, 35, 100783.
- Ibrahim, A. F., Abdelaal, A., & Elkatatny, S. (2022). Formation resistivity prediction using decision tree and random forest. *Arabian Journal for Science and Engineering*, 47(9), 12183–12191.
- IS 2720, Part—7. (1980). Methods of test for soils: determination of water content-dry density relation using light compaction. New Delhi: Bureau of Indian Standards.
- IS 2720, Part—4. (1985). Methods of test for soils: grain size analysis. New Delhi: Bureau of Indian Standards.

- IS 2720, Part—13. (1986). Methods of tests for soils: direct shear test. New Delhi: Bureau of Indian Standards.
- Ishibashi, I., & Zhang, X. (1993). Unified dynamic shear moduli and damping ratios of sand and clay. *Soils and Foundations*, 33(1), 182–191.
- Kumar, Y., Trivedi, A., & Shukla, S. K. (2023a). Damage evaluation in pavement-geomaterial system using finite element-scaled accelerated pavement testing. *Transportation Infrastructure Geotechnology*. <https://doi.org/10.1007/s40515-023-00309-y>
- Kumar, Y., Trivedi, A., & Shukla, S. K. (2023b). Deflections governed by the cyclic strength of rigid pavement subjected to structural vibration due to high-velocity moving loads. *Journal of Vibration Engineering and Technology*. <https://doi.org/10.1007/s42417-023-01063-8>
- Kumari, N., & Trivedi, A. (2022). The effect of confined granular soil on embedded pzt patches using fft and digital static cone penetrometer (DSCP). *Applied Sciences*, 12(19), 9711.
- Li, D., Wang, Y., Yan, W. J., & Ren, W. X. (2021). Acoustic emission wave classification for rail crack monitoring based on synchrosqueezed wavelet transform and multi-branch convolutional neural network. *Structural Health Monitoring*, 20(4), 1563–1582. <https://doi.org/10.1177/1475921720922797>
- Liu, S., Wang, L., Zhang, W., Sun, W., Fu, J., Xiao, T., & Dai, Z. (2023). A physics-informed data-driven model for landslide susceptibility assessment in the Three Gorges Reservoir Area. *Geoscience Frontiers*, 14, 101621.
- Mehra, S., & Trivedi, A. (2021). Pile groups subjected to axial and torsional loads in flow-controlled geomaterial. *International Journal of Geomechanics*, 21(3), 04021002.
- Mohan, R., Gupta, A., & Gaur, K. (2021). Utilization of Bitumen, Aggregate and Wax with Rubber Tyre in a Flexible Pavement. In IOP Conference Series: Materials Science and Engineering (Vol. 1197, No. 1, p. 012017). IOP Publishing. <https://doi.org/10.1088/1757-899X/1197/1/012017>
- Myles, A. J., Feudale, R. N., Liu, Y., Woody, N. A., & Brown, S. D. (2004). An introduction to decision tree modeling. *Journal of Chemometrics: A Journal of the Chemometrics Society*, 18(6), 275–285.
- Ojha, S., & Trivedi, A. (2013). Shear strength parameters for silty-sand using relative compaction. *Electronic Journal of Geotechnical Engineering*, 18(1), 81–99.
- Phoon, K. K., & Zhang, W. (2023). Future of machine learning in geotechnics. *Georisk Assessment and Management of Risk for Engineered Systems and Geohazards*, 17(1), 7–22.
- Quinlan, J. R. (1993). C4. 5 Programs for Machine Learning. Morgan Kaufmann, San Mateo, California.
- Quinonero-Candela, J., & Rasmussen, C. E. (2005). A unifying view of sparse approximate Gaussian process regression. *The Journal of Machine Learning Research*, 6, 1939–1959.
- Rodriguez-Galiano, V., Sanchez-Castillo, M., Chica-Olmo, M., & Chica-Rivas, M. J. O. G. R. (2015). Machine learning predictive models for mineral prospectivity: An evaluation of neural networks, random forest, regression trees and support vector machines. *Ore Geology Reviews*, 71, 804–818.
- Safavian, S. R., & Landgrebe, D. (1991). A survey of decision tree classifier methodology. *IEEE Transactions on Systems, Man, and Cybernetics*, 21(3), 660–674.
- Sagi, O., & Rokach, L. (2018). Ensemble learning: A survey. *Wiley Interdisciplinary Reviews: Data Mining and Knowledge Discovery*, 8(4), e1249.
- Seed, H. B., Wong, R. T., Idriss, I. M., & Tokimatsu, K. (1986). Moduli and damping factors for dynamic analyses of cohesionless soils. *Journal of Geotechnical Engineering*, 112(11), 1016–1032.
- Sharma, S., Venkateswarlu, H., & Hegde, A. (2019). Application of machine learning techniques for predicting the dynamic response of geogrid reinforced foundation beds. *Geotechnical and Geological Engineering*, 37, 4845–4864.
- Singh, M., Trivedi, A., Shukla, S.K. (2020a). Effect of geosynthetic reinforcement on strength behaviour of sub-grade-aggregate composite system. In: Sustainable Civil Engineering Practices. pp. 61–70. https://doi.org/10.1007/978-981-15-3677-9_7
- Singh, M., Trivedi, A., & Shukla, S. K. (2020b). Influence of geosynthetic reinforcement on unpaved roads based on CBR, and static and dynamic cone penetration tests. *International Journal of Geosynthetics and Ground Engineering*, 6(2), 1–13. <https://doi.org/10.1007/s40891-020-00196-0>
- Singh, M., Trivedi, A., & Shukla, S. K. (2020c). Fuzzy-based model for predicting strength of geogrid-reinforced subgrade soil with optimal depth of geogrid reinforcement. *Transportation Infrastructure Geotechnology*, 7(4), 664–683. <https://doi.org/10.1007/s40515-020-00113-y>
- Swain, P. H., & Hauska, H. (1977). The decision tree classifier: Design and potential. *IEEE Transactions on Geoscience Electronics*, 15(3), 142–147.
- Wilson, A. G., Knowles, D. A., & Ghahramani, Z. (2011). Gaussian process regression networks. *arXiv preprint arXiv:1110.4411*
- Xu, M., Watanachaturaporn, P., Varshney, P. K., & Arora, M. K. (2005). Decision tree regression for soft classification of remote sensing data. *Remote Sensing of Environment*, 97(3), 322–336.
- Yang, E. K., Choi, J. I., Kwon, S. Y., & Kim, M. M. (2011). Development of dynamic py backbone curves for a single pile in dense sand by 1g shaking table tests. *KSCCE Journal of Civil Engineering*, 15, 813–821.
- Younas, N., Ali, A., Hina, H., Hamraz, M., Khan, Z., & Aldahmani, S. (2022). Optimal causal decision trees ensemble for improved prediction and causal inference. *IEEE Access*, 10, 13000–13011.
- Zhang, N., Xiong, J., Zhong, J., Leatham, K. (2018). Gaussian process regression method for classification for high-dimensional data with limited samples. <https://doi.org/10.1109/ICIST.2018.8426077>
- Zhang, W., Gu, X., Tang, L., Yin, Y., Liu, D., & Zhang, Y. (2022). Application of machine learning, deep learning and optimization algorithms in geoenvironment and geoscience: Comprehensive review and future challenge. *Gondwana Research*, 109, 1–17.
- Zhang, W., Li, H., Li, Y., Liu, H., Chen, Y., & Ding, X. (2021). Application of deep learning algorithms in geotechnical engineering: A short critical review. *Artificial Intelligence Review*, 54, 5633.

Publisher's Note

Springer Nature remains neutral with regard to jurisdictional claims in published maps and institutional affiliations.